Publishing House
AKAPIT

COMPUTER METHODS IN MATERIALS SCIENCE
Informatyka w Technologii Materiałów

Vol. 17, 2017, No. 3

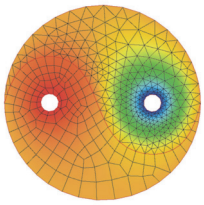

MULTI-SCALE MODELING OF DEPOSITION AND RE-SPUTTERING OF Ni_xTi_{1-x} THIN FILM IN A MAGNETRON SPUTTERING CHAMBER

ANIRUDDHA DEY[1], SHAMPA AICH[2], SUDIPTO GHOSH[3], S. S. MOHAPATRA[4], A. KUMAR[5], *AJIT BEHERA[6]

[1]*Tata steel, Jamshedpur-831001, India*
[2,3]*Department of Metallurgical and Materials Engineering, Indian Institute of Technology, Kharagpur-721302, India.*
[4,5]*Department of Chemical Engineering, National Institute of Technology, Rourkela-769008, India*
[5]*Department of Chemical Engineering, Indian institute of technology, Dhanbad-826004, India*
[6]*Department of Metallurgical and Materials Engineering, National Institute of Technology, Rourkela-769008, India*
**Corresponding author email: beheraajit@nitrkl.ac.in*

Abstract

Deposition and re-sputtering of Ni-Ti thin films by magnetron sputtering was simulated using a multi-scale modeling approach. The sputtering of Ni and Ti targets and the transport of sputtered Ni and Ti atoms through the background gas were simulated using a Monte-Carlo approach, while the deposition of the sputtered atom onto the film surface was analyzed using molecular dynamics. The interaction of Ar^+ ions with the deposited film under the influence of substrate bias was also simulated using a Monte-Carlo approach. The distribution of sputtered atoms over the substrate and the fraction of total sputtered atoms from Ni and Ti targets that reached the substrate were calculated for an off centred target which made an angle of 30° with the substrate. The effects of target voltage and gas temperature on the distribution of sputtered atom over substrate were studied with the help of the aforesaid simulations. It was observed that with increasing target voltage, the fraction of sputtered atoms reaching the substrate was increased slightly for a pure Ni target, while it showed very little change for a pure Ti target. With increasing gas temperature, the value for the same decreased initially, but increased beyond a critical temperature. The velocities of incident Ni and Ti atoms on the substrate were calculated and it was found that no intrinsic re-sputtering could take place for a $Ni_{0.5}Ti_{0.5}$ thin film under the simulated conditions. The fraction of deposited atoms that were re-sputtered by Ar^+ ions under varying substrate bias was also calculated and was found to increase substantially with the increase in the magnitude of the substrate bias voltage. Finally, the stability of crystalline and amorphous Ni and Ti were estimated on the basis of fraction of atoms re-sputtered using a classical molecular dynamics approach.

Key words: NiTi; sputtering; re-sputtering; Multi-scale modeling; thin films

1. INTRODUCTION

Ni-Ti thin films are important from an engineering perspective mainly because of their shape-memory effect, psedoelasticity and bio-compatibility which potentially makes them candidates for varied applications including Micro-Electro-Mechanical Systems (MEMS) and as vascular implants (Sanjabi & Barber, 2010; Burow et. al., 2008; farenite et. al., 2005; Habijan et. al., 2012). Even though Ni-Ti thin films have been made using sputtering techniques for over two decades now, the control and under-

ISSN 1641-8581

standing of the parameters that influence the thin film properties are yet to be understood in their entirety.

Process parameters play significant role in the proper synthesis of desired Ni-Ti films (Fu et. al., 2001; Fua et. al., 2004). The shape memory transition temperature range for a shape memory alloy is extremely sensitive to its composition and structure (Kok et.al., 2016) which in turn depends on several process parameters like sputtering voltage, substrate temperature, substrate bias (Li et.al., 2006; Priyadarshini et. al., 2013; Eswarraju et. al., 2008). In the past, the shape-memory effect and pseudo-elasticity, as exhibited by Ni-Ti alloys, have been experimented upon (Burow et.al., 2008) and modeled successfully (Savi et. al., 2002). However, only a few studies on the effect of the aforementioned parameters on Ni-Ti thin film deposition and growth have been studied in depth through the help of models and simulations. Abhilash et al. (Abhilash et. al., 2005) had simulated the sputtering of mosaic Ni-Ti targets and documented the effects of varying background gas pressure and substrate to target distance. Priyadarshini et al. (Priyadarshini et.al., 2013) had studied the effects of re-sputtering on the crystallinity of Ni-Ti thin films using classical molecular dynamics simulations.

In this paper, we have developed a multi-scale approach for the simulation of deposition and re-sputtering of Ni-Ti thin films within a magnetron sputtering chamber. Using Monte Carlo simulation the fluxes of Ni and Ti atoms on the substrate were estimated and the values of the fluxes were fed to a classical molecular dynamics based model, which simulated the collision of Ni and Ti adatoms with the surface of the deposited film. The effect of substrate bias on the re-sputtering yield of Ni-Ti thin film was studied using another Monte-Carlo approach. The flux of Ar^+ ions near reaching the target and the substrate (under the application of a substrate bias) was estimated and this was used to calculate the fraction of atoms that will be lost due to the effect of re-sputtering.

2. MULTI-SCALE MODELING OF MAGNETRON SPUTTERING DEPOSITION

In our attempt to simulate a complex physical process like sputtering we had to use a multi-scale approach where the length scale varied from 10^{-10} m to 10^{-1} m. Monte-Carlo simulation was carried out at a higher length scale to model the transport of Ni and Ti atoms from target to substrate while molecular dynamics simulation was performed at nano-scale (in the vicinity of the film surface). Monte-Carlo simulations were also carried out at the nano-scale to model the sputtering and re-sputtering. For our simulation, we had to make a few assumptions which have been justified in several earlier reports (Sambandama et. al., 2005; Senthilnathan et.al., 1998; Eisenmenger-Sittner et.al., 1995).

(a) The concentration of the sputtered atoms is less as compared with the concentration of the background gas atoms.
(b) All ions from the plasma impinge normally onto the target surface.
(c) Sputtered species are electrically neutral.
(d) Mutual collisions of sputtered atoms from different targets do not take place.
(e) The collision between the sputtered atoms and the background gas atoms are elastic in nature
(f) Collisions with charged species are neglected.
(g) Background gas pressure and temperature is spatially uniform.
(h) The sticking coefficient is 1 for the substrate and the walls of the sputtering chamber.

For convenience, we have divided the whole simulation into three uniquely identifiable parts and discussed the physics behind their simulation separately: Sputtering of Ni and Ti atoms from the target, their transport to the substrate/deposited film and subsequent collision of the adatoms with the surface of the deposited film.

A. Sputtering of Ni and Ti atoms from the target

The nascent energy and spatial distribution of the particles sputtered from the target is a necessary input for the simulation that we have carried out. This distribution varies with the target voltage, bombarding species and target material species. To this effect, the initial distribution can be obtained theoretically, using the Monte-Carlo method based on Thompson distribution.

The energy distribution of the sputtered species may be assumed to follow the Thompson distribution which is given by (Thompson et.al., 2002):

$$\Phi(E) \approx \frac{E}{(E+U_s)^{3-2m}} dE \qquad (1)$$

where $\Phi(E)$ is the population density function (of energy, E), and U_s is the surface binding energy. The ion energy in the magnetron

sputtering chamber is low and the value of m is set to zero. This distribution extends to infinity, and therefore cut-off energy has to be defined. The expressions provided by Zhang et al. (Zhang et.al., 2004) can be used to describe the nascent angular distribution of the sputtered atoms.

$$Y(E,\theta)\sim|\cos\theta|\left[1-\frac{1}{4}\sqrt{\frac{E_{th}}{E}}\gamma(\theta)\right] \quad (2)$$

where,

$$Y(\theta)=\frac{3\sin^2\theta-1}{3\sin^2\theta}+\frac{\cos^2\theta(3\sin^2\theta-1)}{2\sin^3\theta}ln\frac{1+\sin\theta}{1_{\sin\theta}} \quad (3)$$

Y(E,θ) is the angular distribution for the sputter yield, θ is the ejection angle, E_{th} is the threshold energy for sputtering. Matsunami et al. (Matsunami et.al., 1984) suggested the formula for the threshold energy:

$$\frac{E_{th}}{U_s}=1.9+3.8\left(\frac{M_2}{M_1}\right)^{-1}+0.134\left(\frac{M_2}{M_1}\right)^{1.24} \quad (4)$$

where M_1 is the mass of the incident atom and M_2 is the mass of target atom.

B. Transport of sputtered atoms to substrate

Once a sputtered atom is created, the next step is to follow its journey as it navigates through the background gas atoms and moves towards the different part of the magnetron sputtering unit. During this, the sputtered atoms undergo collisions (assumed to be elastic) with the background gas atoms and consequently there is a change in its direction of motion and velocity at every collision. Thus, at each collision, in order to find the new direction of motion and velocity, one has to establish equations for conservation of momentum and energy.

This is arrived at by using the following approach:

(a) Based on Equation 1, 2, 3 and 4, the initial phase space of the sputtered atom is stochastically assigned.

(b) Each of these atoms sputtered from the target travels a distance λ before colliding with a background gas atom. The length of the free path λ can be calculated stochastically using standard Monte Carlo method which gives $\lambda=|\lambda_m\ln(x)|$ where x is a random number between 0 and 1.

From kinetic gas theory (McDaniel et. al., 1964), the mean free path λ_m can be calculated as:

$$\frac{1}{\lambda_m}=\sqrt[4]{2\pi}\frac{P_s}{kT}{r_s}^2+\pi\frac{P_g}{kT}\left(r_s+r_g\right)^2\left(1+\frac{M_s}{M_g}\right)^{\frac{1}{2}} \quad (5)$$

where, P_s and P_g are the partial pressures, and r_s and r_g are the atomic radius of the sputtered atom and gas species, respectively. It is assumed that the concentration of sputtered atoms is much less as compared to the background gas atoms and thus the first term of the above equation may be neglected. It has also been shown in literature (Wagner et.al., 1980) that this mean free path is also dependent on energy and an empirical fit gives the following expression:

$$\frac{1}{\lambda_m}=E^{-a}\pi\frac{P_g}{kT}\left(r_s+r_g\right)^2\left(1+\frac{M_s}{M_g}\right)^{\frac{1}{2}} \quad (6)$$

where, E is the energy of the sputtered atom and a is a parameter such that for E less than 1eV, a=0 and E greater than 1eV, a=0.29.

(c) The change in the velocity and the direction of motion is computed on the basis of the equation proposed by Goldstein (Goldstein, 1950) for a classical scattering problem.

$$\theta_{cm}=\Pi-2\int_{R_0}^{\infty}\frac{pdR}{R^2\left[1-\frac{p^2}{R^2}-\frac{U(R)}{E_{CM}}\right]^{\frac{1}{2}}} \quad (7)$$

where θ_{cm} is the centre of mass scattering angle, p is the impact parameter, R_0 is the value of R for which the denominator of the integral becomes zero, U(R) is the interaction potential that exists between the two colliding particles, and E_{cm} is the energy of the incident atom with respect to the center of mass. The impact parameter P and R_0 are related by the following equation:

$$p^2={R_0}^2[1-\frac{U(R)}{E_{cm}}] \quad (8)$$

E_{cm} is related to the incident atom energy E by

$$E_{cm}=\frac{{M_T}/{M_P}}{1+{M_T}/{M_P}}E \quad (9)$$

where M_T and M_P are the masses of the target and the projectile species. Thus one can calculate the scattering angles θ_{cm} for different energy values E and given interaction potentials U(R).

The interaction potential U(R) has a direct bearing on the scattering angle θ_{cm}. The interaction potential between two atoms can be described in general as:

$$U(R)=\frac{Z_1Z_2E^2}{R}\phi(\frac{R}{a}) \quad (10)$$

where Z_1 and Z_2 are the atomic numbers of the two interacting atoms, E is the charge of an electron and

Φ is a screening function which helps in incorporating the effect of the electrons in the coulombic potential that exists between the nuclei of the two atoms under consideration.

The interaction potential with an attractive part shows the same general dependence as purely repulsive potentials (Barry et.al., 2014) when we consider for the ranges, reflection coefficients and the sputtering yield of the projectile energy and angle of incidence. Thus we can safely use one of the many completely repulsive interaction potentials that exist in the scientific literature.

For our simulation we have used the Moliere potential which is given by (Eckstein et.al., 1992):

$$U(R) = \frac{Z_1 Z_2 e^2}{R}[0.35e^{-bR} + 0.55e^{-4bR} + 0.10e^{-20bR}] \quad (11)$$

where $b = (0.3/a_f)$ and a_f is Firsov screening length given by:

$$a_f = 0.8853 a_b \left[Z_1^{-\frac{1}{2}} + Z_2^{-\frac{1}{2}}\right]^{-\frac{2}{3}} \quad (12)$$

where a_b is the Bohr radius.

C. Collision of Ni and Ti adatoms and Ar+ ions with the film surface

1. *Collision of Ar^+ ions with the film surface*

The collision of Ar^+ ions with the film surface under the influence of a substrate bias was simulated by using a Monte-Carlo algorithm similar to the one described above. The mechanism of collision and transport of the ion through the deposited film had been described by Biersack et al (Biersack and Eckstein, 1984).

The re-sputtering phenomenon is understood by analyzing collision cascades. When the incident atom undergoes a collision with Ni or Ti atom of the film, that atom recoils with some kinetic energy. Subsequent collisions of this primary recoil and its daughters with other stationary Ni and Ti atoms lead to the formation of the collision cascade. Atoms close to the surface, which are a part of a collision cascade, may acquire sufficient energy to overcome the surface binding energy of the material and escape from the surface leading to the formation of a re-sputtered atom. This surface binding energy may be approximated by identifying it with the sublimation energy of the target.

The flux of the Ar^+ ions over the substrate under the influence of a substrate bias was calculated using the following equation:

$$N_{Ar^+} = \rho_{Ar^+}\sqrt{\frac{2E}{M_{Ar}}} \quad (13)$$

where N_{Ar} is the number flux of the Ar^+ ions, ρ_{Ar^+} is the number density of Ar^+ ions near the substrate for the given geometry of the sputtering chamber, E and M_{Ar} are the energy and mass of the Ar^+ ions respectively. Since, E is directly proportional to $\sqrt{V}$, where V is the magnitude of the target/substrate voltage, we can deduce the following relation:

$$\frac{N^S{}_{Ar^+}}{N^T{}_{Ar^+}} = k\sqrt{\frac{V^S}{V^T}} \quad (14)$$

where $N^S{}_{Ar^+}$ and $N^T{}_{Ar^+}$ are the number fluxes of Ar^+ions near the substrate and target respectively and k is the parameter that depends on the nature of the distribution of electric and magnetic fields inside the sputtering unit. The value of $N^T{}_{Ar^+}$ was calculated by comparing simulated and experimental results.

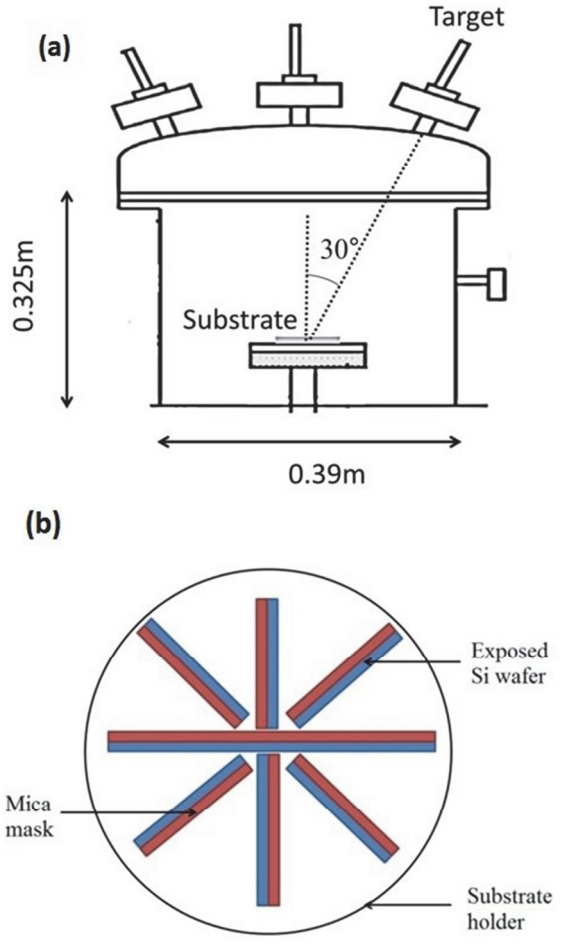

Fig. 1. *experimental set-up for NiTi deposition:* ***(a)*** *the magnetron sputtering chamber,* ***(b)*** *the substrate arrangement inside the chamber.*

2. *Collision of Ni and Ti atoms with the film surface*

The collision of Ni and Ti adatoms with the stationary Ni and Ti atoms of the deposited film was simulated through classical molecular dynamics. For our simulation, we have used the Embedded Atom model (EAM) potential (http://lammps.sandia.gov, 2015) which is given by:

$$E_i = F_\alpha\left(\sum_{i\neq j}\rho\beta(r_{ij})\right) + \frac{1}{2}\sum_{i\neq j}\phi_{\alpha\beta}(r_{ij}) \quad (15)$$

where r_{ij} is the distance between atoms i and j, $\phi_{\alpha\beta}$ is a pair-wise potential function, $\rho\beta$ is the contribution to the electron charge density from atom j of type β at the location of atom i, and F is an embedding function that represents the energy required to place atom i of type α into the electron cloud.

Classical molecular dynamics (CMD) is a deterministic approach which reveals the evolution of the phase space of atoms. It thus reveals more information than stochastic Monte-Carlo simulation. However, the collision of Ar^+ ions with film surface cannot be simulated with CMD due to the lack of reliable Ar^+-NiTi interaction potential.

3. *Stability of crystalline phase in re-sputtered film*

The creation of significant vacancies in a thin film will result in destabilization of crystalline structure. Earlier studies using classical molecular dynamics have revealed that beyond a critical percentage of vacancies, the crystalline phase does not remain stable. This has been attributed to sever distortion in the structure due to the presence of a large number of vacancies. Priyadarshini et al. (Priyadarshini et.al., 2013) carried out CMD simulation to study the stability of crystalline phase in the Ni_x-Ti_{1-x} thin film under 0 to 10 % of vacancy. They observed that, although crystalline $Ni_{0.4}Ti_{0.6}$ with 5 % vacancy transform to the amorphous phase, pure Ni and pure Ti remained crystalline up to 10 % vacancy. The present work extends the vacancy concentration up to which the crystallinity is preserved to 20 %, following the same approach. The simulation methodology for the same is described in the next section.

D. Simulation Methodology

For the simulation of the sputtering process, a Monte-Carlo simulator SIMTRA (Aeken et.al., 2008; http://www.draft.ugent.be/, 2015), which is based on the aforesaid theories, was used in conjunction with the TRIM (Transport of Ions in Matter) module of SRIM (Stopping and Range of Ions in Matter) (www.srim.org, 2015).

The Monte-Carlo simulation was carried out for 106 sputtered particles (Ni or Ti) for a specific geometry of a magnetron sputtering unit as shown in Figure (1a). The target to substrate distance was fixed at 0.125 m while the angle that the normal to the planar target made with the normal to the circular substrate was 30º. The target thickness was 0.003 m while the radius of the circular target was 0.0381 m. For the simulation, the circular substrate was divided into a square 65X65 grid and the data for each grid was stored.

Following the Monte-Carlo simulation, which gave us the distribution so f atom and their velocities as they reach the substrate, the MD modeling was done using LAMMPS (http://lammps.sandia.gov, 2015) to numerically integrate the equations of motion. This simulator utilizes the velocity-verlet algorithm to numerically integrate the equations of motion. In order to achieve this, a 50 ÅX50ÅX50Å film having the uniform composition of 50 % Ni and 50 % Ti, was generated and consequently bombarded with impinging atoms having velocities as obtained from the Monte-Carlo simulation.

In the present study, MD simulations were also carried out to understand the effect of vacancy creation resulting from re-sputtering on the relative stability of crystalline and amorphous phases. The large-scale atomistic/molecular massively parallel simulator mentioned above (http://lammps.sandia.gov, 2015), was used to carry out the MD simulations. The simulation box, having the dimension of 100ÅX100ÅX100Å with approximately 62,500 atoms was equilibrated at 300 K and subjected to periodic boundary condition. Different percentages of vacancies were generated by randomly removing atoms from the simulation box. After removal of vacancies, the periodic configuration was annealed and the radial distribution function (RDF) of the resulting atomic arrangement was plotted.

The interaction of incident Ar^+ with the film surface was studied with the help of TRIM (Transport of Ions in Matter) (Biersack and Eckstein, 1984) for 106 incident ions and varying substrate bias voltages and thin film composition.

3. EXPERIMENTAL PROCEDURE

The Ni-Ti thin film was developed on a Si(100) substrate, which was arranged as shown in Figure (1b), by using a DC magnetron sputtering machine having the geometry for which simulations were carried out. In the sputtering chamber, Ni and Ti target (each of radius 0.0381 m) were positioned at a distance of 0.125 m from the substrate and the angel of 30º as shown in Figure (1a). The film deposition parameters are given in Table I. Each of them was equipped with controlled shutters to avoid cross-contamination. Prior to deposition process, the p-type Si substrate was clean thoroughly with DI water and rinsed with 2% HF solution. For measurement of thickness, the half portion of the required position of the sample covered with mica (Figure (1b)). A constant flow of carrier gas Ar (99.999%) was controlled with a leak valve. Before each run during sputtering, the targets have been pre-sputtered for 2 minutes in order to ascertain the same state of the targets in every run. The thickness of the film was calculated by surface profilometry (Dektak 150, Arizona).

Table I. *Experimental parameters.*

Parameters	Values
Partial pressure of gas (Ar)	0.67 Pa
Gas flow rate:	50 SCCM
Substrate to target distance	0.125 m
Substrate temperature	300 K
Substrate bias voltage	0 V
Substrate rotation	0 rpm
Target voltage	300 V
Deposition time	30 min

4. RESULTS AND DISCUSSION

The sputtering process had been simulated using the aforesaid methodology to study the effect of gas temperature and target voltage on the distributions and velocity of Ni and Ti atoms over the substrate and also quantitatively estimate the magnitude of re-sputtering taking place. The results obtained are discussed below.

A. Target sputtering

The mean sputtering angle and mean sputtering energy of atoms as they were sputtered from the target by impinging gas ions and the sputter yield are compared in Table II and Table III for both Ni and Ti targets at varying target voltages.

Table II. *Mean sputtering angle, mean sputtering energy and sputter-yield of Ni target for varying target voltage.*

	Ni target voltage				
	100V	200V	300V	400V	500V
Mean sputtered atom energy (eV)	18.58	21.40	22.97	24.37	25.14
Mean ejection angle (w.r.t normal in degrees)	147.63	148.24	148.55	148.64	148.83
Sputter-yield	0.5131	0.9304	1.2900	1.6100	1.9000

Table III. *Mean sputtering angle, mean sputtering energy and sputter-yield of Ti target for varying target voltage.*

	Ti target voltage				
	100V	200V	300V	400V	500V
Mean sputtered atom energy (eV)	19.87	24.63	28.22	31.14	33.76
Mean ejection angle (w.r.t normal in degrees)	147.58	147.37	147.33	147.23	147.15
Sputter-yield	0.1806	0.3295	0.4501	0.5483	0.6361

The mean sputtered atom energy is the average energy with which an atom of the target species is ejected out of the target. The mean ejection angle is the average angle that the sputtered atoms make with respect to the target surface such that the normal to the target surface is directed towards the target. By this definition, atoms coming out normally and away from the target would have an ejection angle of 180 degrees while an atom going normally into the target would have an ejection angle of 0 degree. The sputter-yield is the average number of target species that is sputtered out by one incident atom.

The obtained values of the sputtering yields bear good co-relation with the experimental values that found by Laegreid et al. (Laegreid et.al., 1961).

The energy with which a Ti atom is sputtered is much higher compared to that of Ni atoms and consequently, shows a lower sputter yield. This observation can be attributed to the fact that Ti is less dense than Ni and thus a larger fraction of the incident energy is transferred directly to a Ti atom. However, the mean ejection angle of the sputtered atom from the target is nearly the same for both Ni and Ti as both have a similar value of sublimation energy.

B. Distribution of atoms over substrate

For the given geometry of the sputtering unit, the distribution of the sputtered atoms that reach the substrate was obtained for both Ni and Ti target sputtering for the same target geometry, target voltage, and gas temperature. For validating the predicted distribution of adatoms on the substrate, sputter deposition of Ni was carried out. The sputtering parameters, namely, Ar pressure, target to substrate distance, target voltage type of magnetron source, were identical to those for which simulation in the present study was carried out. Figure (2a) shows the relative distribution of Ni on Si(100) substrate and experimentally measured thickness are superimposed on the contour plot. A reasonably good match between the simulated and experimental distribution can be observed.

Comparing the distributions obtained for Ni and Ti atoms for the sputtering of an equal number of atoms of each species, we observed that in the case of Ni target sputtering, the number of atoms in the region close to the target is more as compared to that of Ti target sputtering under identical simulation conditions for sputtering. The distribution of Ni and Ti atoms sputtered separately has been compared using contour plot sin Figure (2b). It should be noted that this distribution did not consider the effect of substrate rotation, which is usually used to ensure that the distribution of atoms is not skewed towards the region close to the target overtime.

C. Effect of target voltage

Only a fraction of all sputtered atoms reached the substrate and it showed little variation with the target voltage, at a fixed gas temperature (300 K) and pressure (0.67 Pa) as illustrated by Table IV.

1. Effect on particle distribution over substrate

The distribution of sputtered atoms over the substrate varies with the target voltage. Effect of very high target voltage was not studied as the present simulation does no account for the influence of target heating which becomes very significant at high voltages. The variation in the distribution of Ni atoms over the substrate with target voltage has been shown in Figure (3a), from which we can infer that an increase in target voltage causes the slight increase in the number of sputtered atoms reaching the target. Though such a conclusion could have been arrived at intuitively as well, this simulation helped us to measure the increase quantitatively.

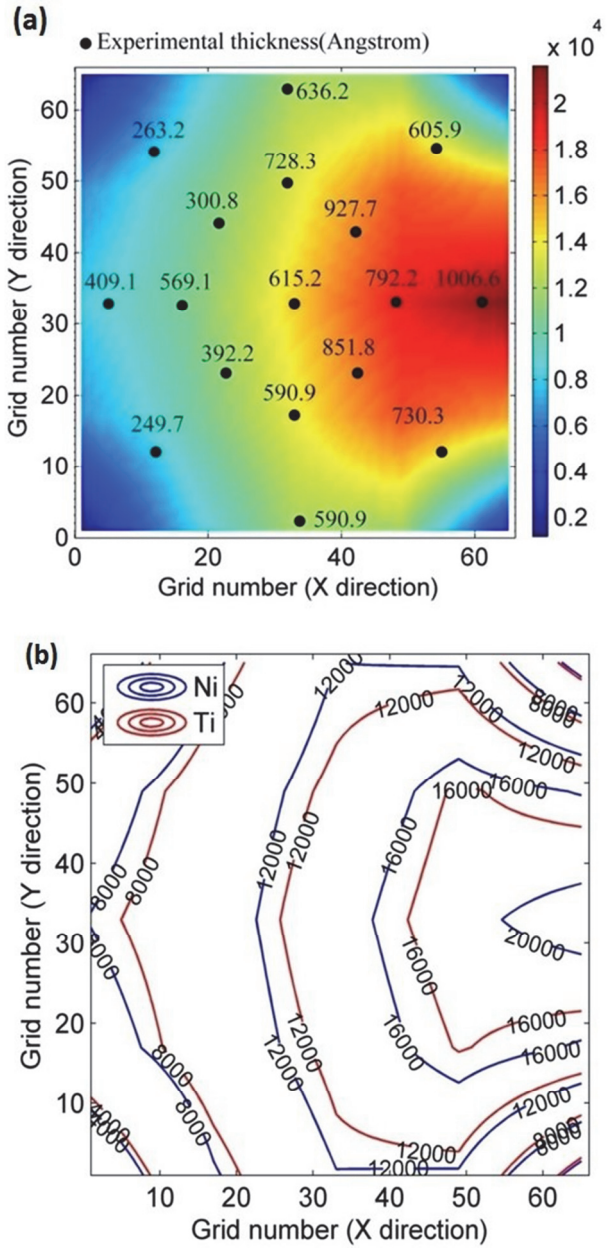

Fig. 2. *Particle Distribution of atoms over substrate at target voltage = 300 V, gas pressure = 0.67 Pa and gas temperature = 300 K. (a) the relative distribution of Ni on Si(100) substrate, (b) Particle Distribution of Ni and Ti over the substrate.*

Table IV. *Variation of the fraction of sputtered atom reaching the substrate with target voltage.*

	Target voltage				
	100V	300V	400V	500V	800V
Percentage of Ni atoms reaching substrate	26.33	27.07	27.17	27.28	27.41
Percentage of Ti atoms reaching substrate	25.18	25.15	25.15	25.13	25.13

2. *Effect on adatom velocity*

With increasing target voltage, the energy with which an atom escapes the target is higher and consequently the velocity with which this sputtered atom reaches the substrate is also higher. We observe from Figure (4a) that the particle velocity for Ti atom is much higher than what has been observed for Ni atom and the rate of increase of the particle velocity with target voltage is much higher for Ti atoms as compared to Ni atoms.

Table V. *Comparison with experimental measurement of adatom velocity.*

Parameters	In this paper	Britun et al. (Britun et.al., 2008)	Britun et al. (Britun et.al., 2011)
Magnetron source	Stationary	Moving	-
Target diameter	0.762m	0.10m	0.10 m
Ar partial pressure	5mTorr	≥0.5mTorr	5 and 20 mTorr
Substrate to target dist	0.125m	0.015m	0.015,0.045, and 0.070 m
Target voltage:	300V	200-400V	Power avg./pulse=12kW
Velocity	-	Tiavg.vel.≈2km/s	Tivel.≈1-2km/s
Method used	-	Planar Fabry-Perot interferometer	Laser-induced fluorescence

Very few experiments have been carried out to measure the velocity of Ni and Ti Adatoms in magnetron sputtering chamber. Table V presents the findings of these experiments.

It is nearly impossible to accurately compare our simulated data with experimental data available in the literature as most of these experiments have been carried in sputtering chambers having geometries different from ours. However, by comparing the data given in Table V and the average particle velocity reported in Figure (4a), we can conclude that there exists an order of magnitude match between the reported experimental data and our model's prediction.

D. Effect of gas temperature

The effect of gas temperature, at a fixed target voltage (300 V) and gas pressure (0.67 Pa), on the fraction of sputtered atoms reaching the substrate is illustrated in Table VI.

Table VI. *Variation of the fraction of sputtered atom reaching the substrate with gas temperature.*

	Gas Temperature					
	300K	400K	500K	600K	700K	1000K
Percentage of Ni atoms reaching substrate	27.13	26.50	26.22	25.85	25.90	26.06
Percentage of Ti atoms reaching substrate	25.15	24.92	24.78	24.75	24.82	25.28

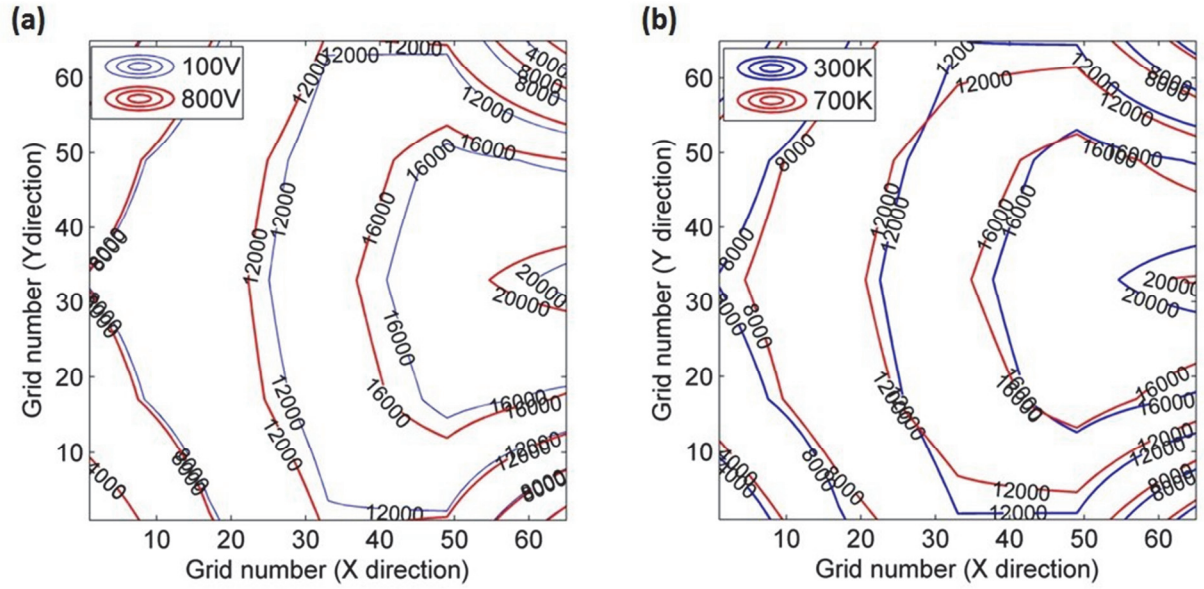

Fig. 3. *Variation of particle distribution of Ni over the substrate showing:* ***(a)*** *Effect of target voltage,* ***(b)*** *Effect of gas temperature.*

The percentage of sputtered atoms reaching the substrate initially decreases and then increases beyond a critical temperature. To understand this, we must consider the fact that with increasing temperature the mean free path increases and trajectories of atoms from the target to the substrate become straighter. An increase in the mean free path not only decreases the number of atoms reaching the substrate with the help of collisions with the background gas but also increases the number of atoms that reaches the substrate unhindered by collisions with the background gas atoms. Till a critical temperature is reached, the former dominates while beyond it, the latter phenomenon plays the more significant role.

4. Effect on particle velocity

With increasing gas temperature, the mean free path of the sputtered atoms increases and thus they encounter a less number of collisions and consequently lose less energy during their journey from the target to the substrate (Britun et.al., 2011). We observe from Figure (4a) that the particle velocity for Ti atoms is much higher than that of Ni atoms and the rate of Increase of the particle velocity with gas temperature is only slightly higher for Ti atoms as compared to that of Ni atoms.

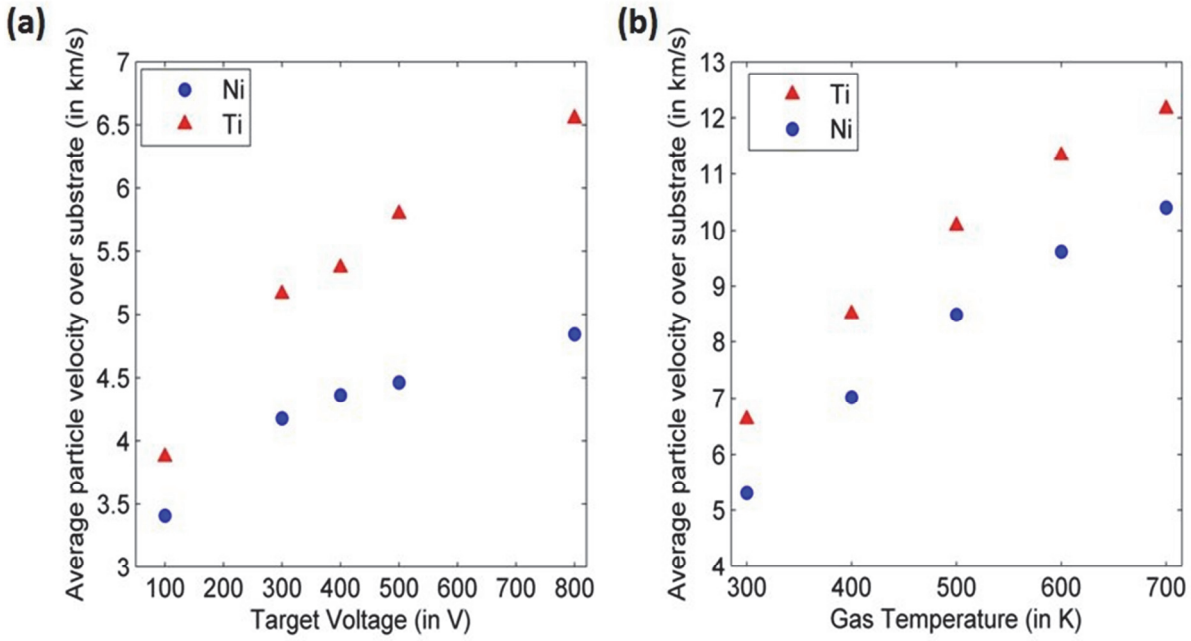

Fig. 4. *Particle velocity of sputtered Ni and Ti atoms over substrate.* ***(a)*** *Effect of target voltage.* ***(b)*** *Effect of gas temperature.*

3. Effect on particle distribution over substrate

As observed from Figure (3b), for the given geometry of the sputtering unit, with the increase in temperature, the number of sputtered atom reaching the central portion of the substrate increases while the peripheral regions of the substrate record a decrease in the number of sputtered atom reaching those areas. This observation can be explained by the fact that with increasing temperature the mean free path increases and as a result more atoms tend to move in a linear path from the target to the substrate. Thus, regions which are directly in the line of sight of the target receive more atoms than other regions.

E. Simulation of re-sputtering

Re-sputtering from the surface of the deposited film can be caused either by the adatoms themselves or by incident Ar^+ ions that strike the film surface under the influence of substrate bias (Gregoire et.al., 2007).

1. Re-sputtering caused by Ni and Ti adatoms

It was observed that the energy associated with the flux of Ni and Ti adatoms were not sufficient to cause re-sputtering from the surface of the deposited film and all sputtered atoms that reached the substrate, for the given target voltages (200 V-800 V)

and temperatures (300 K-700 K), were incorporated inside the Ni-Ti film. Therefore, it can be concluded that the re-sputtering upon the application of negative substrate bias is due to the bombardment of Ar^+ ions.

2. *Re-sputtering caused by Ar^+ ions*

The value of N^T_{Ar+} was calculated by using experimental and simulated data. Knowing the fraction of sputtered atoms that reach the substrate and the sputter yield of the target for a given target voltage, the number of Ar^+ ions that would need to strike the target to produce a film of given thickness can be calculated. In a sputtering chamber, having the geometry used in the simulation, sputtering and deposition of Ni were carried out for a period of 20 minutes at a target voltage of 300 V. The average thickness of the resultant film obtained was 74.34 nm. Using this experimental data, N^T_{Ar+} was calculated to be 3.24×1019 $m^{-2}s^{-1}$. By using Equation 14 and assuming a value for k, N^S_{Ar+} was calculated for varying substrate bias voltages. The value of k can be expected to lie between 0 and 0.5 considering the facts that the target has a higher voltage than the substrate and that behind the target lies the magnetron, which concentrates the Ar^+ ions near the target.

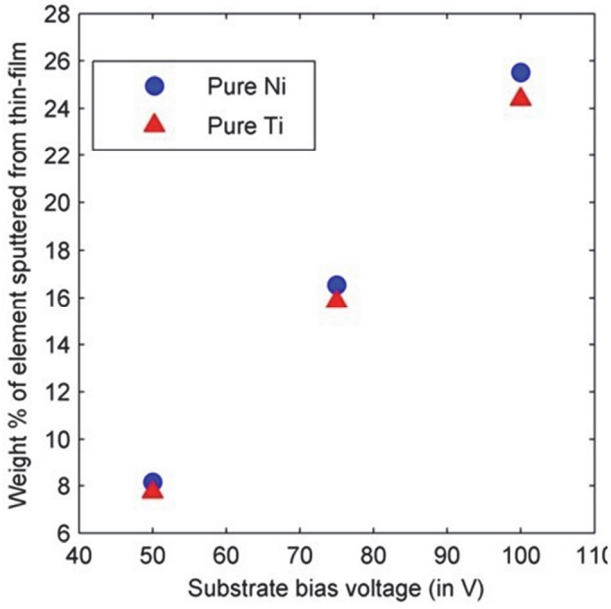

Fig. 5. *Variation of the fraction of material lost due re-sputtering from pure Ni and Ti films at varying substrate bias voltages.*

Using the aforementioned calculation and an assumed valued of k =0.3, the fraction of material lost due re-sputtering from pure Ni and Ti films has been shown in Figure (5).

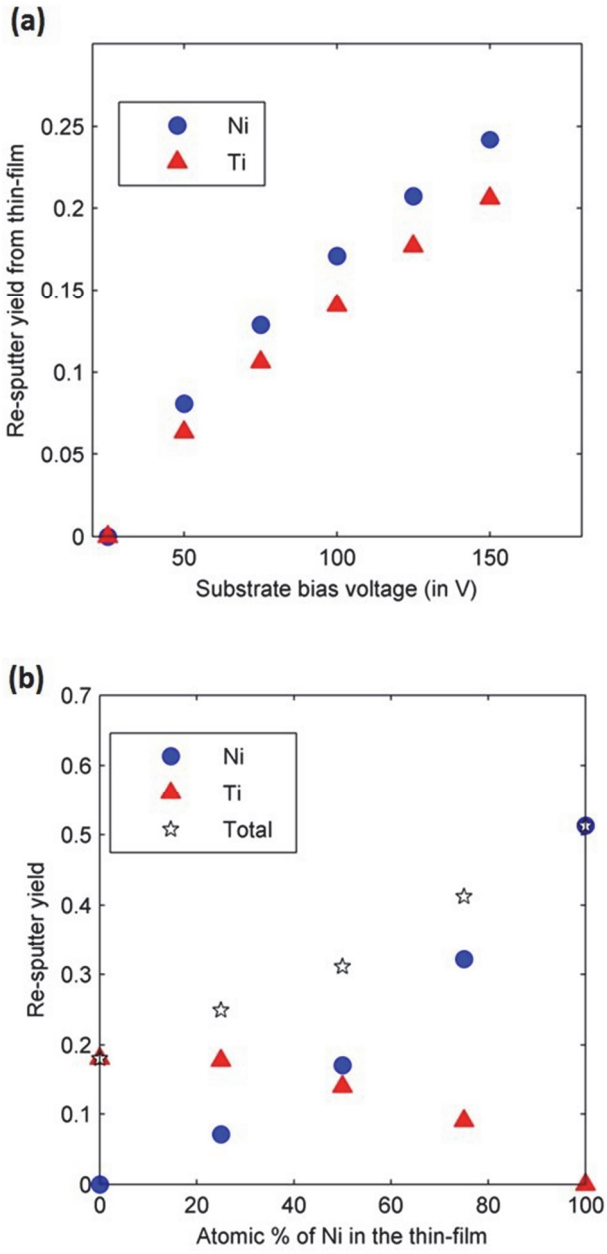

Fig. 6. *Variation of re-sputter yield with substrate bias voltage and thin film composition for a 100 nm thickness film.*

The variation of re-sputter yield for varying substrate bias voltages is shown in Figure (6a) while the variation of the same (at a fixed substrate bias voltage = 100 V) with thin film composition is shown in Figure (6b).

We observe that only beyond a critical substrate bias voltage can re-sputtering take place.

5. PREDICTION OF FILM CRYSTALLINITY

From Figure (6a), it can be concluded that the fraction of Ni atoms ejected out as a result of re-

sputtering (i.e. re-sputtering yield) is ~0.12 for a substrate bias of -90 V. The number of atoms ejected due to re-sputtering is equal to the number of vacancies generated in the deposited film due to re-sputtering. For Ti, the fraction of vacancy generated when substrate bias equals -90 V is ~0.10. The results of classical molecular dynamics based simulation of structural change in Ni crystals as a result of 10 % and 20 % vacancy creation is shown with a help of a radial distribution function plot in Figure (7a) and Figure (7b), respectively. Similar results were also obtained for Ti. From the RDF plots obtained from our simulation, it is apparent that both Ni and Ti thin films would be crystalline in nature when deposited at -90 V substrate bias.

6. CONCLUSIONS

Through the simulation of magnetron sputtering for the synthesis of Ni-Ti thin films, we were able to make the following inferences:

(a) For the given geometry of the sputtering unit, the average number of Ni atoms that reached the substrate was 2 % more as compared to the same of Ti atoms under identical experimental conditions.

(b) On an average, the velocity with which sputtered Ti atoms reach the substrate is 25 % higher than that of Ni atoms.

(c) With the increase in target voltage, the percentage of sputtered atoms reaching the target slightly increases.

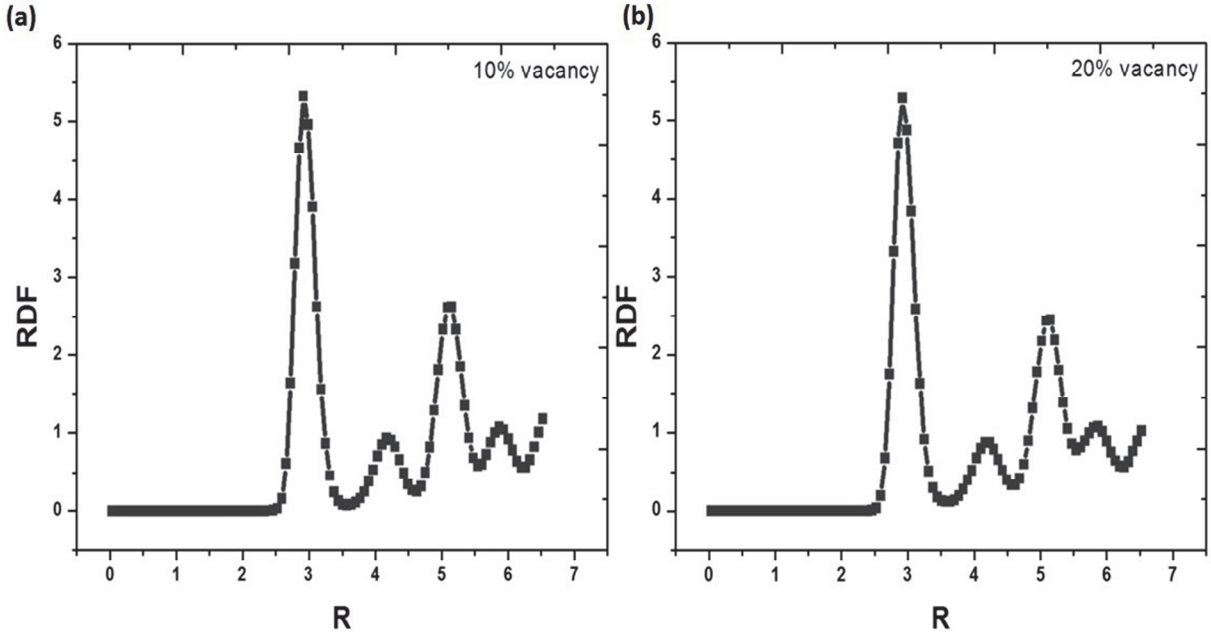

Fig. 7. *Radial distribution function (RDF) plot for Ni crystal with different vacancy percentage.*

Glancing incidence X-ray diffraction (GIXRD) plots, high resolution transmission electron microscopy (HRTEM) images, and selected area diffraction (SAD) patterns of Ni and Ti films deposited at the substrate bias of -90 V, reported by Priyadarshini et al. [9] further attests the crystallinity of the films at a substrate bias of -90 V as suggested by our model. Thus, although direct measurement of vacancy concentration or the re-sputtering yield for Ni and Ti films are not available, the indirect evidence (GIXRD and HRTEM results) suggest that the estimated magnitude of the re-sputtering yield obtained from our simulation is within acceptable error margins.

(d) With increasing background gas temperature, the percentage of sputtered atoms reaching the substrate decrease still a critical temperature is reached, beyond which it increases.

(e) The rate of increase in particle velocity with temperature is nearly the same in the case of Ni and Ti atoms over the temperature range in which the simulations were carried out.

(f) The velocity with which the sputtered atoms reach the target changes with the target voltage and this change is considerably more prominent in the case of Ti atoms.

(g) For the given sputtering parameters, no intrinsic re-sputtering can take place for Ni-Ti thin films.

(h) Significant loss in weight of the thin film was observed due to re-sputtering caused by Ar^+ ions in the presence of substrate bias voltage.

For better accuracy in the sputtering deposition, re-sputtering is an essential factor in optimization of the sputtering parameter. Henceforth, the future improvement of NixTi1-x thin film for MEMS will be concentrated on re-sputtering in sputtering technique.

REFERENCES

Abhilash, V., Sumesh, M. A., Mohan, S., 2005, Composition analysis of NiTi thin films sputtered from a mosaic target: synthesis and simulation, *Smart Mat. Struct.,* 14, 323-328.

Barry, P. R., Philipp, P., Wirtza, T., Kieffer, J., 2014, Mechanisms of silicon sputtering and cluster formation explained by atomic level simulations, *J. Mass Spectrom,* 49, 185-194.

Biersack, J. P., Eckstein, W., 1984, Sputtering studies with the Monte Carlo Program TRIM.SP, *J. Appl. Phys. A*, 34, 73-94.

Britun, N., Han, J. G., Oh, S. G., 2008, Velocity distribution of neutral species during magnetron sputtering by Fabry–Perot interferometry, *Appl. Phys. Lett.,* 92, 141503, DOI:10.1063/1.2907505.

Britun, N., Palmucci, M., Snyders, R., 2011, Fast relaxation of the velocity distribution function of neutral and ionized species in high-power impulse magnetron sputtering, *Appl. Phys. Lett.*, 99, 131504.

Britun, N., Palmucci, M., Snyders, R., 2011, Fast relaxation of the velocity distribution function of neutral and ionized species in high-power impulse magnetron sputtering, *Appl. Phys. Lett*., 99, 131504. DOI:10.1063/1.3644989.

Burow, J., Prokofiev, E., Somsen, C., Frenzel, J., Valiev, R. Z., Eggeler, G., 2008, Martensitic transformations and functional stability in ultra-fine grained NiTi shape memory alloys, *Materials Science Forum*, 584, 852.

Burow, J., Prokofiev, E., Somsen, C., Frenzel, J.,. Valiev, R. Z, Eggeler, G., 2008, Martensitic Transformations and Functional Stability in Ultra-Fine Grained NiTi Shape Memory Alloys, *Materials Science Forum*, 584-586, 852-857.

Eckstein, W., Hackel, S., Heinemann, D., Fricke, B., 1992, Influence of the interaction potential on simulated sputtering and reflection data, *Z. Phys. D, Atoms, Molecules and Clusters*, 24, 171-176.

Eisenmenger-Sittner, C., Beyer Knecht, R., Bergauer, A., Bauer, W., Betz, G., 1995, Angular distribution of sputtered neutrals in a post magnetron geometry: Measurement and Monte Carlo simulation, *Journal of Vacuum Science & Technology A: Vacuum, Surfaces, and Films*, 13, 2435-2443.

Eswar Raju, K. S., Bysakh, S., Sumesh, M. A., Kamat, S. V., Mohan, S., 2008, The effect of ageing on microstructure and nanoindentation behaviour of dc magnetron sputter deposited nickel rich NiTi films, *Mat. Sci. Eng. A,* 476, 267-273.

Fu, Y. Q., Huang, W. M., Du, H. J., Huang, X., Tan, J. P., Gao, X. Y., 2001, Characterization of TiNi shape-memory alloy thin films for MEMS applications, *Surf. Coat. Technol*., 145, 107-112.

Fua, Y., Du, H., Huang, W., Zhang, S., Hu, M., 2004, TiNi-based thin films in MEMS applications: a review, *Sens. Actua. A*, 112, 395-408.

Goldstein, H., 1950, *Classical Mechanics*, Addisen Wesley Publishing Co, 3rd ed.

Gregoire, J. M., Lobovsky, M. B., Heinz, M. F., DiSalvo, F. J., van Dover, R. B., 2007, Resputtering phenomena and determination of composition in codeposited films, *Phy. Rev. B*, 76, 195437, DOI: 10.1103/Phys Rev B.76.195437.

Habijan, T., DeMiranda, R. L., Zamponi, C., Quandt, E., Greulich, C., Schildhauer, T. A., Koller, M., 2012, The biocompatibility and mechanical properties of cylindrical NiTi thin films produced by magnetron sputtering, *Mat. Sci. Eng. C*, 32, 2523-2528.

Kok, M., Dagdelen, F., Aydoğdu, A., Aydogdu, Y., 2016, The change of transformation temperature on NiTi shape memory alloy by pressure and thermal ageing, Journal of Physics: Conference Series, *9th International Conference on Magnetic and Superconducting Materials (MSM15)*, IOP Publishing, 667, 012011, DOI:10.1088/1742-6596/667/1/012011

Laegreid, N., Wehner, G. K., 1961, Sputtering Yields of Metals for Ar^+ and Ne^+ Ions with Energies from 50 to 600 ev, *Journal of Applied Physics,* 32, 365, DOI: http://dx.doi.org/10.1063/1.1736012.

LAMMPS Molecular Dynamics Simulator, available online at: http://lammps.sandia.gov., accessed: 23.11.2017.

Li, M. Y. H., Li, L. M., Meng, F. L., Zheng, W. T., Zhao, J., Wang, Y. M., 2006, Effect of substrate temperature on the surface and interface oxidation of NiTi thin films, *J. Elect. Spect. Rel. Phenom*., 151, 144-148.

Matsunami, N., Yamamura, Y., Itikawa, Y., Itoh, N., Kazumata, Y., Miyagawa, S., Morita, K., Shimizu, R., Tawara, H., 1984, Energy dependence of the ion-induced sputtering yields of monatomic solids, *Atomic Data and Nuclear Data Tables*, 31, 1-80.

McDaniel, E. W., 1964, *Collision phenomena in ionized gases*, Wiley Seriesin Plasma Physics, Wiley, New York.

Priyadarshini, B. G., Gupta, M. K., Ghosh, S., Chakraborty, M., Aich, S., 2013, Role of substrate bias during deposition of magnetron sputtered Ni, Ti and Ni-Ti thin films, *Surf. Eng*., 29, 689, DOI: 10.1179/1743294413Y.0000000182

Sambandama, S. N., Bhansalia, S., Bhethanabotlab, V. R., Sood, D. K. , 2006, Studies on sputtering process of multicomponent Zr-Ti-Cu-Ni-Be alloy thin films, *Vacuum*, 80, 406-414.

Sanjabi, S., Barber, Z. H., 2010, The effect of film composition on the structure and mechanical properties of NiTi shape memory thin films, *Surface and Coatings Technology*, 204, 1299-1304.

Sanjabi, S., Cao, Y. Z., Sadrnezhaad, S. K., Barber, Z. H., 2005, Binary and ternary NiTi-based shape memory films deposited by simultaneous sputter deposition from elemental targets, *J. Vac. Sci. Technol. A*, 23, 1425-1429.

Savi, M. A., Paiva, A., Baeta-Neves, A. P., Pacheco, P. M. C.L., 2002, Phenomenological modeling and numerical simulation of shape memory alloys: a thermo-plastic-phase transformation coupled model, *Journal of Intelligent Material Systems and Structures*, 13(220), 261-273.

Senthilnathan, S., Mohan Rao G., Mohan, S., 1998, Fluid simu-simulation of a pulsed-power inductively coupled argon plasma, *J. Vac. Sci. Technol. A*, 84, 564-571.

Simulation of Metal Transport, available online at: http://www.draft.ugent.be/, accessed: 23.11.2017.

SRIM, Stopping and range of ions in materials can be downloaded from, available online at: www.srim.org, accessed: 23.11.2017.

Thompson, M. W., 2002, Atomic collision cascades in solids, *Vacuum*, 66, 99-114.

Van Aeken, K., Mahieu, S., 2008, The metal flux from a rotating cylindrical magnetron: a Monte Carlo simulation, *Journal of Physics D: Applied Physics*, 41, 205307, DOI: 10.1088/0022-3727/41/20/205307.

Wagner, C. D., Davis, L. E., Riggs, W. M., 1980, The energy dependence of the electron mean free path, *Surf. Interface Anal*., 2, 53-55.

Zhang, Z. L., Zhang, L., 2004, Anisotropic angular distribution of sputtered atoms, *Plasma Sci. Plasma Technol*., 159, 301, DOI: 10.1080/10420150410001724495.

WIELOSKALOWE MODELOWANIE OSADZANIA I PONOWNEGO ROZPYLANIA CIENKIEJ WARSTWY Ni_xTi_{1-x} W MAGNETRONOWEJ KOMORZE NAPYLAJĄCEJ

Streszczenie

Osadzanie i ponowne rozpylania cienkiej warstwy Ni_xTi_{1-x} w magnetronowej komorze napylającej było symulowane z zastosowaniem modelowania wieloskalowego. Rozpylanie Ni i T oraz transport rozpylanych atomów przez gaz w komorze symulowano metodą Monte Carlo, a osadzanie rozpylanych atomów na powierzchni cienkiej warstwy analizowano za pomocą metody dynamiki molekularnej. Oddziaływanie jonów Ar^+ z osadzoną warstwą z uwzględnieniem wpływu nachylenia podłoża symulowano również metodą Monte Carlo. Rozkład osadzanych atomów na podłożu i ułamek osadzonych atomów Ni i Ti które osiągnęły podłoże dla przesuniętego celu nachylonego pod kątem 30^o do podłoża. Na podstawie wykonanych symulacji oceniono wpływ napięcia w komorze i temperatury gazu na rozkład osadzonych atomów. Zaobserwowano, że wraz ze wzrostem napięcia dla celu z czystego Ni wzrasta nieznacznie ułamek rozproszonych atomów, które osiągnęły cel. Ten wpływ jest pomijalny dla czystego Ti. Wraz ze wzrostem temperatury wspomniany ułamek początkowo maleje a następnie powyżej temperatury krytycznej zaczyna wzrastać. Obliczone zostały prędkości atomów Ni i Ti osiągających podłoże i zauważono, że ponowne rozpylanie w warunkach symulacji dla cienkiego filmu Ni0.5Ti0.5 nie jest możliwe. W dalszej kolejności obliczono ułamek osadzonych atomów, które zostały ponownie rozpylone przez jony Ar^+ dla różnego nachylenia podłoża. Zaobserwowano, że wzrost wielkości napięcia podłoża znacznie zwiększa ten ułamek. W końcowej części pracy na podstawie oceny ułamka atomów ponownie rozpylonych określono stabilność krystalicznego i amorficznego Ni i Ti wykorzystując do tego celu metodę dynamiki molekularnej.

Received: May 22, 2017
Received in a revised form: September 12, 2017
Accepted: October 25, 2017